ISSN 1063-7761, Journal of Experimental and Theoretical Physics, 2014, Vol. 119, No. 3, pp. 479–487. © Pleiades Publishing, Inc., 2014.
Original Russian Text © D.A. Balaev, A.A. Krasikov, A.A. Dubrovskii, S.V. Semenov, O.A. Bayukov, S.V. Stolyar, R.S. Iskhakov, V.P. Ladygina, L.A. Ishchenko, 2014, published in Zhurnal Eksperimental'noi i Teoreticheskoi Fiziki, 2014, Vol. 146, No. 3, pp. 546–556.

ORDER, DISORDER, AND PHASE TRANSITION IN CONDENSED SYSTEM

Magnetic Properties and the Mechanism of Formation of the Uncompensated Magnetic Moment of Antiferromagnetic Ferrihydrite Nanoparticles of a Bacterial Origin

D. A. Balaev[a,b]*, A. A. Krasikov[b], A. A. Dubrovskii[a], S. V. Semenov[a,b], O. A. Bayukov[a], S. V. Stolyar[a,b], R. S. Iskhakov[a], V. P. Ladygina[c], and L. A. Ishchenko[b]

[a] *Kirenskii Institute of Physics, Siberian Branch, Russian Academy of Sciences, Akademgorodok, Krasnoyarsk, 660036 Russia*

**e-mail: dabalaev@iph.krasn.ru*

[b] *Siberian Federal University, Svobodnyi pr. 79, Krasnoyarsk, 660041 Russia*

[c] *International Scientific Center of Extreme States of Organisms, Krasnoyarsk Scientific Center, Siberian Branch, Russian Academy of Sciences, Akademgorodok 50, Krasnoyarsk, 660036 Russia*

Received February 12, 2014

Abstract—The magnetic properties of the superparamagnetic ferrihydrite nanoparticles that form as a result of the vital activity of *Klebsiella oxytoca* bacteria are studied. Both an initial powder with an average number of iron atoms $N_{Fe} \sim 2000–2500$ in a particle and this powder after annealing at 140°C for 3 h in air are investigated. The following substantial modifications of the magnetic properties of the ferrihydrite nanoparticles are detected after annealing: the superparamagnetic blocking temperature increases from 23 to 49.5 K, and the average magnetic moment of a particle increases (as follows from the results of processing of magnetization curves). The particles have antiferromagnetic ordering, and the magnetic moment resulting in the superparamagnetism of the system appears due to random spin decompensation inside the particle. For this mechanism, the number of uncompensated spins is proportional to the number of magnetically active atoms raised to the one-half power, and this relation holds true for the samples under study at a good accuracy. The possible causes of the detected shift of magnetic hysteresis loops at low temperatures upon field cooling are discussed.

DOI: 10.1134/S1063776114080044

1. INTRODUCTION

Nanoparticles with antiferromagnetic (AF) ordering exhibit magnetic properties that differ substantially from the properties of analogous bulk materials [1–4]. First of all, this is the presence of uncompensated magnetic moment μ_{unc}. Néel predicted three possible causes of the appearance of μ_{unc} in an AF particle [5]. They are random breaks in an AF order, i.e., partial spin decompensation of magnetically active atoms on the particle surface (case 1) or throughout the particle volume (case 2), and an odd number of planes with parallel spins (case 3). The uncompensated magnetic moment of an AF particle depends on the number of atoms N having magnetic moment J as follows:

$$\mu_{unc} \approx JN^b, \quad (1)$$

where N is the number of atoms and exponent b is 1/3, 1/2, and 2/3 for cases 1, 2, and 3, respectively. The value of μ_{unc} begins to play a key role in the magnetic properties of particles at $N \lesssim 10^4–10^5$. Uncompensated spins are predominantly ferromagnetically arranged inside a particle, which results in superparamagnetic (SP) behavior of a system of AF particles. The other part of magnetically active atoms, which are antiferromagnetically ordered, manifests itself in the magnetic properties in the form of a linear field response $\chi_{AF}H$, and the values of antiferromagnetic susceptibility χ_{AF} are significantly higher than that of the bulk material. The temperature dependence $\chi_{AF}(T)$ also radically changes: the magnetic susceptibility of a bulk AF material increases with temperature up to the Néel temperature, and the magnetic susceptibility of AF nanoparticles decreases with increasing temperature [1, 6–12]. Relatively small (approximately to 10–20 nm) particles exhibit the blocking temperature below which magnetization curve $M(H)$ is irreversible, which is characteristic of SP systems. Moreover, $M(H)$ hysteresis loops are often shifted upon cooling in an applied magnetic field from a temperature above the blocking temperature [7, 13–21].

Apart from classical oxide AF materials (NiO [13–16], CuO [17, 18], α-Fe_2O_3 [19, 20]), ferritin nanoparticles are being extensively studied [7, 9–12, 22–25]. Ferritin is represented by an AF-ordered ferrihydrite particle inside a protein shell with outside and inside diameters of 12 and 5–8 nm, respectively. This biomaterial is present in almost all living organisms and its function is to store iron. The studies [7, 9–12,

22–25] of the magnetic properties of ferritin nanoparticles were performed on horse spleen ferritin, which is now a commercial product.

Ferrihydrite formed during bacterial synthesis is an analog to ferritin. The nominal formula of ferrihydrite is usually written as $5Fe_2O_3 \cdot 9H_2O$. The energy obtained in the course of the oxidation reaction $Fe^{2+} \longrightarrow Fe^{3+}$ is used by bacteria, and ferrihydrite is "built" as a result of their vital activity. In particular, the nanoparticles of such a material can be formed as a result of the cultivation of *Klebsiella oxytoca* bacteria taken from sediments [26, 27]. Ferrihydrite nanoparticles were comprehensively characterized by various methods [26–30]. The authors of [29] studied the magnetic properties of dried bacterial sediments, which did not exhibit the blocking temperature characteristic of magnetic nanoparticles. As a result of additional cleaning, the authors of [31] prepared a powder containing ferrihydrite nanoparticles, which replicably demonstrated the blocking temperature (about 20 K) and the uncompensated magnetic moment that agrees with Eq. (1) at $b \approx 1/2$. The purpose of this work is to study the modification of the magnetic properties of ferrihydrite nanoparticles undergone by "soft" heat treatment. The annealing temperature was taken to be rather low (140°C), which was determined by the condition of retaining the crystal structure of ferrihydrite (structure transformations occur upon annealing at 300 and 700°C, where ferrihydrite partly transforms into hematite [30]).

2. EXPERIMENTAL

2.1. Sample Preparation

The *Klebsiella oxytoca* strain was extracted from the sapropel in lake Borovoe located in Krasnoyarsk Territory. Microorganisms were inoculated in an agar medium and grown under anaerobic conditions. A stable sol of nanoparticles in an aqueous solution was prepared after multiple ultrasonic treatments of bacterial sediments, centrifugation, and washing, and this sol was then dried. Thus, we studied a powder of magnetic nanoparticles.

This initial powder was designated as sample 1. Part of the powder was held in a drying cabinet at a temperature of 140°C for 3 h in an air atmosphere. It was found that the powder lost about 18% of its mass under these conditions, and it was designated as sample 2.

2.2. Mössbauer Investigations

Since the X-ray diffraction patterns of the prepared powders were characteristic of an amorphous state (see, e.g., [30]), we used Mössbauer spectroscopy to obtain information on the possible changes in the environment of iron or the appearance of other iron oxide phases. Mössbauer studies were performed at room temperature on an MC-1104Em spectrometer with a $^{57}Co(Cr)$ source. Good agreement with the data in [30] was achieved: iron atoms in bacterial ferrihydrite can occupy three sites with different quadrupole splittings. From the standpoint of a local structure, the changes that occurred upon annealing of ferrihydrite nanoparticles were insignificant. The quadrupole splittings and the isomer shifts fell in the range characteristic of various natural iron hydroxides [32].

Thus, we can conclude that no new iron oxide phases formed in bacterial ferrihydrite upon annealing and no substantial changes in the crystal chemistry of the nanoparticle structure took place in it. It is natural to relate the decrease in the sample mass to the loss of intercrystalline water (according to the nominal ferrihydrite formula $5Fe_2O_3 \cdot 9H_2O$, water accounts for 16% of the mass) and partial "burning" of the organic component, in particular, the organic coating of the nanoparticles in the interparticle volume of closely spaced nanoparticles [30].

2.3. Magnetic Measurements

The magnetic measurements were carried out on a vibrating-sample magnetometer [33]. A powder was fixed in paraffin in a measuring capsule, and the data were corrected for the diamagnetic signal from the capsule with paraffin. We used zero field cooling (ZFC) and field cooling (FC) conditions. When hysteretic dependences were measured under FC conditions, a sample was cooled from a temperature of 120 K, which is significantly higher than the blocking temperature.

3. RESULTS AND DISCUSSION

Figure 1a shows the ZFC and FC temperature dependences of the magnetic moment of the powder samples in a field $H = 1$ kOe. The ZFC $M(T)$ dependences have clear maxima at a temperature of about 23 K (initial sample 1) and 49.5 K (annealed sample 2), and the $M(T)$ dependences obtained at different thermomagnetic prehistories diverge at these temperatures. This behavior is characteristic of a system of SP particles with blocking temperature T_B corresponding to the maximum in the ZFC $M(T)$ dependence. Another characteristic feature of the SP system is a significant shift of the blocking temperature toward low temperatures when the applied field increases. The inset to Fig. 1a illustrates this behavior: it presents the values of T_B (axis y) at various applied fields (axis x).

The blocking temperature determined as the maximum in the $M_{ZFC}(T)$ dependence corresponds to the freezing temperature of the largest particles in an applied field. On the other hand, the temperature behavior of the difference between the FC and ZFC magnetic moments ($M_{ZFC} - M_{FC}$) allows us to determine the "average" blocking temperature $\langle T_B \rangle$ (see, e.g., [19]). Figure 1b shows the temperature dependences of the temperature derivative $d(M_{ZFC} -$

$M_{FC})/dT$ for the sample under study. The values of $\langle T_B \rangle$ at $H = 1$ kOe that are determined as the maximum in the dependence $d(M_{ZFC} - M_{FC})/dT$ are 10.5 and 22.4 K for initial sample 1 and annealed sample 2, respectively.

The blocking temperature of the ferrihydrite particles after annealing is seen to increase. According to the generally accepted concepts, T_B is unambiguously related to particle volume V as follows:

$$T_B = KV/\ln(\tau/\tau_0)k \approx KV/25k. \quad (2)$$

Here, K is the magnetic anisotropy constant (specifically, effective magnetic anisotropy related to both the shape anisotropy and the crystalline anisotropy of a particle), k is the Boltzmann constant, and the factor of 1/25 appears because of the ratio of the characteristic measurement time ($\tau \sim 10^2$ s) and particle relaxation time ($\tau_0 \sim 10^{-9}$–10^{-10} s).

As follows from the Mössbauer spectroscopy data (Section 2.2; according to them, no new iron oxide phases appear), either the effective magnetic anisotropy constant of particles K or the particle size (or both parameters) changes. To reveal the causes of the increase in the blocking temperature upon annealing, we consider the magnetization curves of the samples in a temperature range above T_B.

The experimental results are shown in Fig. 2. It follows from these experimental curves that the $M(H)$ dependences are the superposition of an SP contribution, which is described by the Langevin function in the simplest case, and a linear relation $M(H) = \chi_{AF}H$. The linear dependence manifests itself at high fields, where the Langevin function is close to saturation. This behavior was observed for small AF particles [13, 14, 17–19], including analogs of our samples (ferritin nanoparticles) [1, 6–8, 10, 11, 23, 24]. Term $\chi_{AF}H$ describes the canting of the sublattices of the AF core of the particles (χ_{AF} is the magnetic susceptibility of the AF particle core). A comparison of the experimental $M(H)$ dependences of the samples at close temperatures (e.g., 100 and 110 K) demonstrates that the initial increase in the magnetic moment is significantly higher for annealed sample 2 and that the $M(H)$ dependences of the two samples cannot be scaled by the multiplication of the magnetic moment by a coefficient or by subtracting a field-linear $M(H)$ function. This finding indicates that the magnetic moment of a particle in sample 2 is higher than in initial sample 1.

For a quantitative analysis of the $M(H)$ dependences, we use the generally accepted approach for systems of noninteracting AF nanoparticles, where the magnetic moment of a sample is determined by the SP behavior of individual particles with allowance for their size or magnetic moment distribution and by

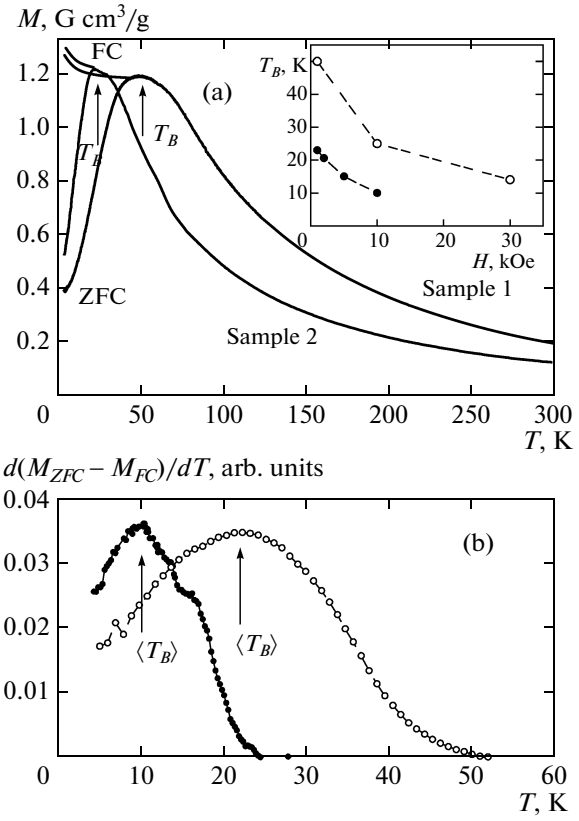

Fig. 1. (a) Temperature dependences of the magnetic moment under ZFC and FC conditions at $H = 1$ kOe for the samples under study. (inset) Blocking temperature T_B vs. the applied field. (b) Temperature dependence of the temperature derivative of $M_{ZFC} - M_{FC}$, the maximum of which determines the average blocking temperature $\langle T_B \rangle$: (●) sample 1 and (○) sample 2.

component $\chi_{AF}H$. In this case, the $M(H)$ dependences are described as follows:

$$M(H) = N_p \int_{\mu_{min}}^{\mu_{max}} L(\mu_p, H) f(\mu_p) \mu_p d\mu_p + \chi_{AF}H. \quad (3)$$

Here,

$$L(\mu_p, H) = \coth(\mu_p H/kT) - 1/(\mu_p H/kT)$$

is the Langevin function, $f(\mu_p)$ is the magnetic-moment distribution function of the particles μ_p, and N_p is the number of particles per unit mass of the powder. We used the lognormal distribution $f(\mu_p) = (\mu_p s(2\pi)^{1/2})^{-1}\exp\{-[\ln(\mu_p/n)]^2/2s^2\}$, where the average magnetic moment of a particle is $\langle \mu_p \rangle = n\exp(s^2)$ and s^2 is the dispersion of $\ln(\mu_p)$. During processing of data at each temperature, we first estimated μ_p without regard for the distribution function to bring the general shape of the $M(H)$ dependences into agreement and then used Eq. (3) to achieve the best agreement between the experimental and fitted curves. We varied $\langle \mu_p \rangle$ and χ_{AF} at various temperatures, while dispersion s^2, which

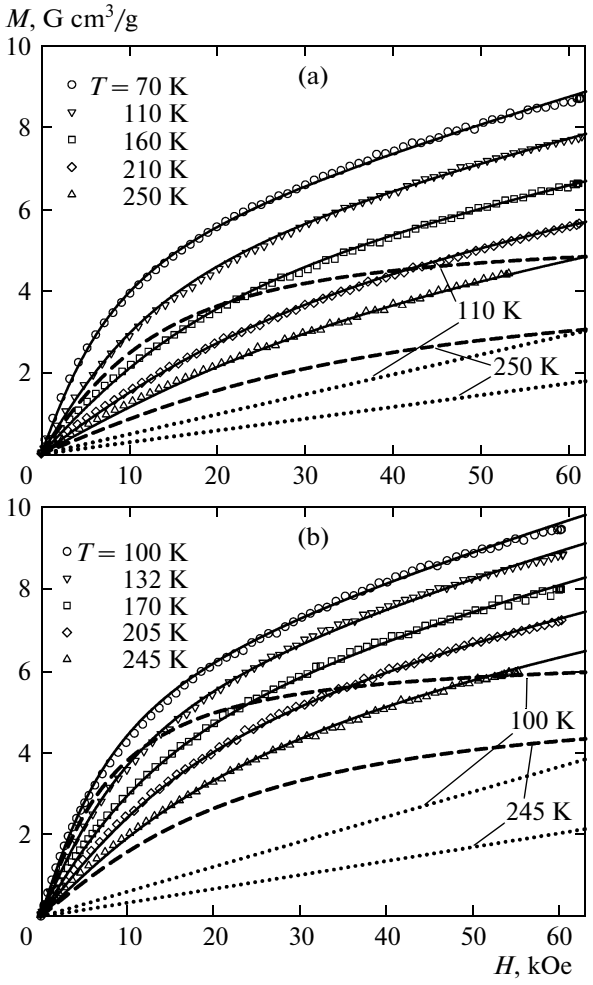

Fig. 2. Isotherms of magnetization curves at various temperatures for (a) initial sample 1 and (b) sample 2 after annealing. (symbols) Experimental points, (solid lines) results of best fitting of $L(H) + \chi_{AF}(H)$ by Eq. (3), (dashed lines) Langevin contribution $L(H)$ (first term in Eq. (3)), and (dotted lines) contribution of the AF component $\chi_{AF}H$ (second term in Eq. (3)) at given temperatures.

characterizes the distribution shape, and the number of particles N_p remained constant.[1] Note that the agreement between the experimental and fitted curves degrades significantly without regard for the distribution function in the field up to 10 kOe, although the adjustable parameters differed by at most 10%.

The solid curves in Fig. 2 illustrate the results of the best fitting. Figures 2a and 2b also show the SP (dashed lines) and AF (dotted lines) contributions for the samples at certain temperatures. Figure 3 shows the temperature dependences of the parameters ($\langle\mu_p\rangle(T)$, $\chi_{AF}(T)$) varied during adjustment. The values of χ_{AF} are approximately the same for both samples,

[1] The values of s^2 were 0.2 and 0.25 and the number or particles was $N_p \approx 2.62 \times 10^{18}$ and 2.2×10^{18} for samples 1 and 2, respectively.

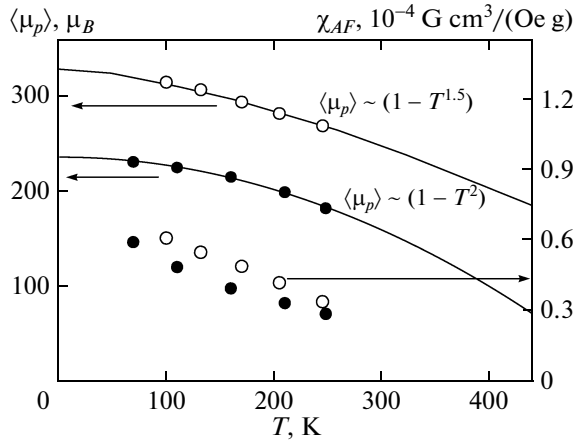

Fig. 3. Average magnetic moment of a particle $\langle\mu_p\rangle$ and χ_{AF} for samples (●) 1 and (○) 2 that was obtained by processing the experimental $M(H)$ curves (Fig. 2) at various temperatures. (solid lines) Dependence (4) at $a = 3/2$ and 2.

and the average magnetic moment of a particle in sample 2 is significantly higher. These findings indicate a larger average particle size in sample 2 and agree with the increase in the blocking temperature (Fig. 1).

We now dwell on the temperature dependence of the average magnetic moment of a particle. It is logical that this dependence for ferro- or ferrimagnetic ordering should obey the well-known Bloch law

$$\langle\mu_p\rangle(T) \sim \langle\mu_p(T=0)\rangle(1 - T^a) \qquad (4)$$

which follows from the existence of "thermal" spin waves, at $a = 3/2$ and sufficiently low temperatures. Indeed, this dependence was observed for SP nanoparticles [34–36]; however, there exists a number of experiments performed on small ferrimagnetic nanoparticles that demonstrated a deviation from the "law of 3/2." In these cases, the exponent is usually higher than 3/2 [37, 38]. In the case of AF ordering, researchers consider the uncompensated magnetic moment of particles. The authors of [10, 11] obtained $a = 2$ in Eq. (4) for ferritin nanoparticles and interpreted this result in terms of the theory of spin waves in antiferromagnets. For the ferrihydrite nanoparticles under study, we found that the $\langle\mu_p\rangle(T)$ dependence follows Eq. (4) at $a = 1.9 \pm 0.1$ for sample 1 (which agrees with the data on ferritin [10, 11]) and at $a = 1.55 \pm 0.05$ for sample 2. This is illustrated in Fig. 3, which shows the results of description of the $\langle\mu_p\rangle(T)$ data by Eq. (4). We can state that, as the ferrihydrite particle size increases, the temperature dependence of the uncompensated magnetic moment changes and becomes closer to the law of 3/2.

The $\langle\mu_p\rangle(T)$ dependence obtained by processing the experimental $M(H)$ dependences can be used to reliably extrapolate the calculated data to $T = 0$ and, hence, to estimate the values of $\langle\mu_p\rangle(T = 0)$, which were found to be $235 \pm 5\mu_B$ and $330 \pm 10\mu_B$ for samples 1 and 2, respectively. If the magnetic moment of the

Fe^{3+} ion is taken to be $J \approx 5\mu_B$, the number of iron ions with uncompensated spins is $N_{unc} \approx 47$ and 65 for samples 1 and 2, respectively. Of course, these estimated values of N_{unc} imply the ideal ferromagnetic orientation of uncompensated spins.

We now compare the calculated values of N_{unc} with the possible versions of formation of an uncompensated magnetic moment in small AF particles. The authors of [28] studied the morphology and structure of the nanoparticles produced by *Klebsiella oxytoca* bacteria, and nanoparticles corresponding to sample 1 were analyzed. As follows from these results, the ferrihydrite particles in sample 1 are elongated cylinders ~3 and 6–7 nm in size. Using these data and the average distance between iron ions in ferrihydrite (3 Å [16]), we can estimate the average number of Fe^{3+} ions in a nanoparticle ($N_{Fe} \sim 2000$–2500). Even at this scatter of the values of N_{Fe}, we obtain $N_{Fe}^{1/2} \approx 45$–50, which coincides with the estimate ($N_{unc} \approx 47$) made from the magnetic data for initial sample 1. This indicates that the uncompensated magnetic moment is induced by random breaks in the spin order throughout the particle volume (including surface; see Eq. (1)). This value ($N_{unc} \approx 47$) is severalfold larger than the value ($N_{unc} \approx N_{Fe}^{1/3} \approx 12$–$14$) expected from the model of uncompensated magnetic moment formation by random breaks in the spin order only on the particle surface.

Note that the relation $N_{unc} \approx N_{Fe}^{1/2}$ holds true for ferrihydrite and ferritin nanoparticles [1, 6–11, 24]. The fact that this relation is rather exactly obeyed is interesting, since the total number of defects, which lead to a break in a spin order, should be on the order of N_{Fe} in this case.[2] However, this is in conflict with the generally accepted approach to these materials as AF particles, which is based on the set of Mössbauer, neutron diffraction, and magnetic studies [1, 4, 6–12, 29]. It is possible that ferrihydrite, which has an imperfect structure, is also characterized by a nonuniform defect distribution over the sublattices [24], and the relation $N_{unc} \approx N_{Fe}^{1/2}$ mainly indicates that defects are present in both the particle surface and volume.

If $N_{unc} \approx N_{Fe}^{1/2}$ and the particle volume is $V \sim N_{Fe}$, we derive the relations $N_{unc1}/N_{unc2} = (V_1/V_2)^{1/2} = (N_{1Fe}/N_{2Fe})^{1/2}$ for particles with different volumes $V_1 \sim N_{1Fe}$ and $V_2 \sim N_{2Fe}$. As a result, we have

$$V_1/V_2 = N_{1Fe}/N_{2Fe} = (N_{unc1}/N_{unc2})^2 = (\mu_{unc1}/\mu_{unc2})^2. \quad (5)$$

[2] At the number of defects on the order of N_{Fe}, the difference between the numbers of defects in both sublattices can be about $N_{Fe}^{1/2}$ from statistical considerations.

When comparing the values of $\langle\mu_p\rangle(T = 0)$ and N_{unc} for the samples under study, we found that the average particle volume in sample 2 increased by $(66/47)^2 \approx 2$ times. This conclusion about an increase in the particle volume can also be drawn from the detected ratio of the blocking temperatures (see Eq. (2)) on the assumption of a constant magnetic anisotropy constant. As follows from Fig. 1, the ratio of the values of T_B at $H = 1$ kOe for these samples is (49.5 K/23 K) ≈ 2.13, and the same value is obtained for the ratio of the average values of $\langle T_B\rangle$ (22.4 K/10.5 K ≈ 2.13; see Fig. 1b). Thus, we found from different data that the particle volume increases about twofold upon annealing.

The conclusion regarding the annealing-induced increase in the nanoparticle volume naturally agrees with the detected mass loss (~18%). Since the annealing temperature is rather low (140°C) and the modification of Mössbauer spectra is insignificant (see Section 2.2), the decrease in the mass of the sample prepared upon drying an aqueous sol is most likely to be related to partial loss of water and the organic shell of particles. During the sublimation of the organic shell of closely spaced nanoparticles, they undergo coalescence, which results in an increase in their average sizes.

Thus, the morphology of the ferrihydrite particles can undergo significant changes at the temperatures slightly above the boiling temperature of water. Of course, these changes should also depend on the medium in which a sample is located. Therefore, it is difficult to determine the Néel temperature from direct magnetization measurements at high temperatures. The authors of [6, 11] proposed to estimate the Néel temperature by extrapolating a $\chi_{AF}(T)$ dependence to the zero value of $\chi_{AF}(T)$.

It is seen in Fig. 3 that, in our case, the antiferromagnetic susceptibility changes approximately according to the law $\chi_{AF}(T) \sim \chi_{AF}(T = 0)(1 - T)$, which is similar to the dependence detected for ferritin nanoparticles in [6, 11]. The linear extrapolation of our $\chi_{AF}(T)$ data in Fig. 3 gives 430 ± 20 K, which agrees with the Néel temperatures obtained for ferritin in [6, 11].

In the range below T_B, the $M(H)$ dependences are hysteretic functions, which is characteristic of SP systems (see Fig. 4, which shows these data for 4.2 K). The bacterial ferrihydrite samples under study are characterized by the following specific features. Up to fields of 60 kOe, the hysteretic $M(H)$ dependences are partial hysteresis loops (see the inset to Fig. 4a). As a consequence, coercive force H_c depends on the maximum applied field H_{max}. For initial sample 1, the values of H_c are 1.5 and 1.9 kOe for $H_{max} = 30$ and 60 kOe, respectively (Fig. 4b). The coercive forces of annealed sample 2 at $H_{max} = 30$ and 60 kOe are slightly higher, 2.35 and 3.6 kOe, respectively (Fig. 4c).

The following rather rare specific feature, which is characteristic of SP system (see [39–42]), is also

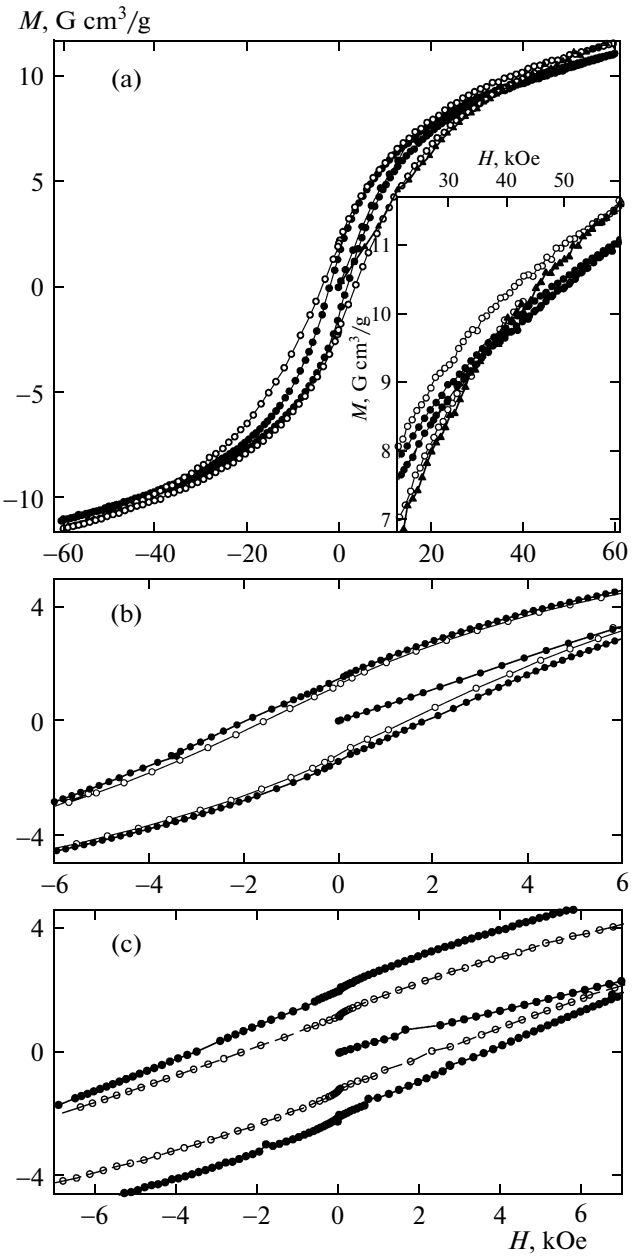

Fig. 4. Hysteretic $M(H)$ dependences at $T = 4.2$ K for samples (○) 1 and (●) 2. (a) Field range of ±60 kOe, maximum applied field $H_{max} = 60$ kOe; (inset) segments of the hysteretic dependences in fields higher than 20 kOe illustrating the irreversibility of the $M(H)$ dependences and the position of the initial magnetization curve relative to the hysteresis loop of sample 2 (▲). (b), (c) Low-field segments of the hysteresis loops at H_{max} = (○) 30 and (●) 60 kOe for samples (b) 1 and (c) 2.

detected: the initial magnetization curve for sample 2 is outside the hysteretic curve in the field range 15–40 kOe (so-called anomalous hysteresis). This feature is illustrated in the inset to Fig. 4a. The difference between the initial magnetization curve and the hysteretic loop exceeds the measurement error, and this effect is repeated after the removal of magnetic prehistory (heating above the blocking temperature). Since we consider an SP system below the blocking temperature, the position of the magnetic moment of a particle is determined by the competition of Zeeman energy $\boldsymbol{\mu}_p \times \mathbf{H}$ and magnetic anisotropy energy KV. This specific feature can result from the existence of numerous close local energy minima of the magnetic moment energy in an anisotropy field [39]. The potential energy minima in which vector $\boldsymbol{\mu}_p$ can be located can be different for the magnetization from the fully demagnetized state and the hysteresis loop section after the cycle $H = 0 \longrightarrow H_{max} \longrightarrow -H_{max} \longrightarrow H = 0$. In this case, we believe that anomalous behavior of the initial magnetization curve can occur (Fig. 4a).

Figure 5a shows the hysteretic $M(H)$ dependences for sample 2, which were obtained under ZFC conditions at $H_{max} = 30$ kOe and upon FC cooling in a magnetic field $H_{FC} = 30$ kOe, on the temperature exceeding the blocking temperature. The hysteresis loop is seen to shift significantly relative to both the abscissa and ordinate axes. Figures 5b and 5c show the detailed $M_{FC}(H)$ dependences for samples 2 and 1 in the region of intersection with the abscissa. Let the field at which the $M_{FC}(H)$ dependence intersects the abscissa be H_{cFC-} and H_{cFC+} for negative and positive values of H, respectively. It is seen that H_{cFC} and H_c differ strongly at negative fields. For samples 1 and 2 at $H_{FC} = 30$ kOe, the values of H_{cFC-} turn out to be −1.93 and −6.2 kOe, and the exchange shift (i.e., the shift of the FC hysteresis loop with respect to the origin of coordinates) determined as $H_S = (H_{cFC-} + H_{cFC+})/2$ is 270 Oe and 2.38 kOe for the samples, respectively. However, after the cycle of measurement of $M_{FC}(H)$ loop from +30 kOe ⟶ −30 kOe ⟶ +30 kOe, the $M(H = +30$ kOe) value does not coincide with $M_{FC}(H = 30$ kOe) obtained under FC conditions. This behavior is illustrated in the inset to Fig. 5a: points A and B correspond to the magnetic moment at $H = 30$ kOe immediately after cooling in this field and after recording a loop under FC conditions. Moreover, if the applied field is decreased at point B, the $M(H)$ dependence does not follow the earlier $M_{FC}(H)$ curve and is close to the segment of the hysteresis loop when the field is decreased (in the range $H > 0$) under ZFC conditions. Point C in Figs. 5a and 5b corresponds to $M(H = 0)$ after recording an $M_{FC}(H)$ loop and decreasing the applied field to zero. Similar behavior is observed for sample 1 (not shown). We can conclude that the FC $M(H)$ hysteresis loop is shifted (which is most pronounced for annealed sample 2); however, this effect becomes less pronounced after the cycle of measuring the $M_{FC}(H)$ dependence.

The shift of the magnetic hysteresis loop of a system of magnetic nanoparticles during field cooling is a frequent phenomenon [1, 13–21, 41, 42], which was observed for ferritin [7, 22] and ferrihydrite [6] nano-

particles. At least two mechanisms are possible for this behavior. The first of them is related to the exchange interaction between surface spins and the core of a particle and is similar to the well-known exchange shift for ferromagnet/antiferromagnet (F/AF) structures [21]. This mechanism can also occur for the spin-glass state of surface spins and ferri- or ferromagnetic ordering in the core [21, 41, 42]. The exchange shift detected for AF nanoparticles, such as NiO [13–16] and CuO [17, 18], is related to the interaction of uncompensated spins with the AF core on the surface. For the exchange shift mechanism in an F/AF structure, H_{EB} is inversely proportional to the magnetization of the F layer and the ferromagnetic layer thickness (this is the surface layer thickness in the case of the spin-glass state of surface spins) [21]. In our case, the relation $N_{unc} \approx N_{\mathrm{Fe}}^{1/2}$ is valid at a high reliability, which supports the fact that the magnetic moment of a particle is formed by both surface spins and the spins in the core of a particle. The mechanism of interaction of such a "ferromagnet" with the AF "matrix" is unclear, and it is difficult to explain the significant increase in H_{EB} (from 270 Oe to 2.38 kOe) for sample 2 (when the average magnetic moment of a particle increases by 1.4 times and the volume increases approximately twofold) in terms of this approach.

Another cause of the detected shift in the hysteresis loop can be the influence of the effective magnetic anisotropy of the particles [22]. Indeed, up to an applied field of 60 kOe, the $M(H)$ dependence remains irreversible and H_c depends on the maximum applied field $H_{\max}$. It is possible that FC conditions are a certain analog of high values of $H_{\max}$ under ZFC conditions and that the observed modification of the hysteresis loop (including the shift of the coercive force, i.e., H_{cFC-}) under FC conditions reflects the high magnetic-anisotropy-induced energy barriers that are overcome by the magnetic moment of a particle. Cycling along the hysteresis loop after field cooling partly "deletes" the magnetic history (see $M(H)$ in segment BC in Fig. 5a). The fact that the initial magnetization curve is outside the hysteresis loop noted above also indicates a complex structure of the energy barriers separating the potential energy minima for vector $\boldsymbol{\mu}_p$ (Fig. 4a).

Thus, apart from the well-known mechanism of exchange interaction between the magnetically ordered phases on the surface and in the core of a particle, the detected shift of a magnetization hysteresis loop under FC conditions can also be related to the effect of the magnetic anisotropy of the particles.

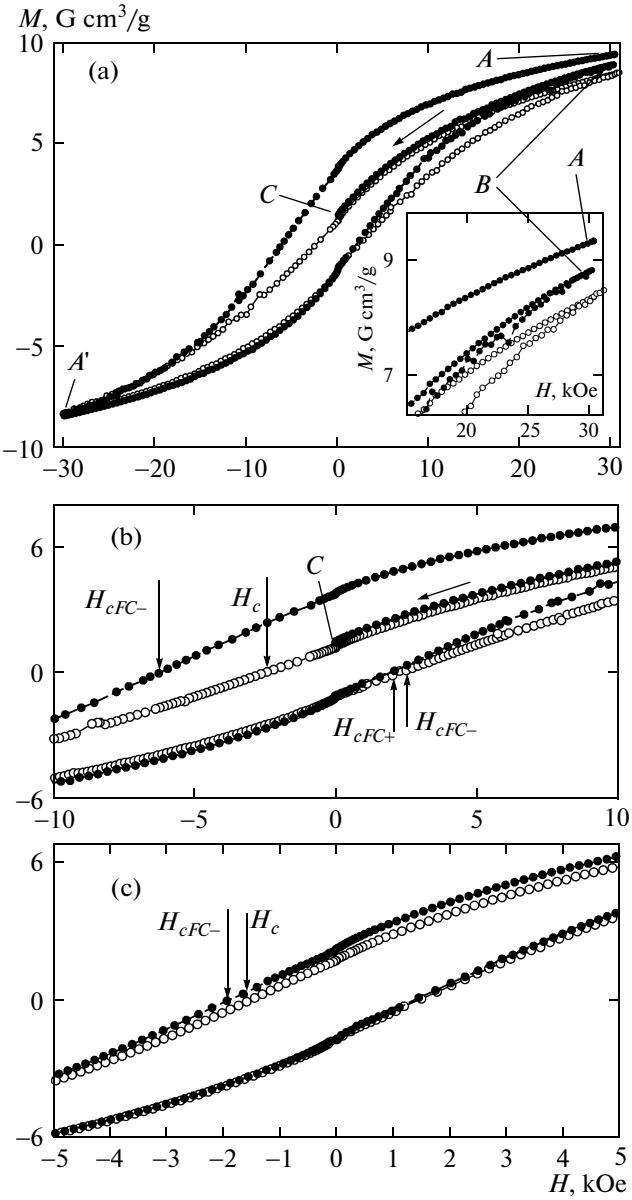

Fig. 5. (a) Hysteretic $M(H)$ dependences at $T = 4.2$ K for sample 2 at $H_{\max} = 30$ kOe under (○) ZFC and (●) FC conditions. The FC $M(H)$ dependence follows the path $A \longrightarrow A' \longrightarrow B \longrightarrow C$. (inset) Segments of these dependences in fields higher than 15 kOe. (b) Low-field segments of the hysteresis loops of sample 2 at $H_{\max} = 30$ kOe under (○) ZFC and (●) FC conditions (H_c, H_{cFC-}, H_{cFC+} are the coercive forces under these conditions, respectively). (c) Low-field segments of the hysteresis loops of sample 1 at $H_{\max} = 30$ kOe under (○) ZFC and (●) FC conditions.

4. CONCLUSIONS

We studied the magnetic properties of the ferrihydrite nanoparticles produced by *Klebsiella oxytoca* bacteria. These nanoparticles exhibit superparamagnetic behavior with a characteristic blocking temperature. Their magnetization curves can be represented as the superposition of a superparamagnetic (Langevin) contribution and an antiferromagnetic component.

Heat treatment of ferrihydrite at $T = 140°C$ for 3 h led to a substantial increase in the blocking temperature (from 23 to 49.5 K), and Mössbauer spectroscopy data showed no radical changes in the environment of iron ions in annealing. An analysis of the magnetization curves with a lognormal distribution of the magnetic moments of particles demonstrated that the average magnetic moment of a particle increases by 1.4 times upon annealing. In combination with the results of earlier investigations of the structure and morphology of the nanoparticles, we concluded that the Néel mechanism of formation of the uncompensated magnetic moment of a particle with antiferromagnetic ordering takes place in them (in both initial and annealed nanoparticles). Specifically, spin decompensation (break in spin order) occurs on the particle surface and in the particle volume and the number of uncompensated spins is $N_{unc} \approx N_{\mathrm{Fe}}^{1/2}$ (where N_{Fe} is the number of magnetically active atoms in a particle). Based on these results, we concluded that the particle size increases approximately twofold upon annealing. The temperature dependence of the uncompensated magnetic moment of small particles (sample 1) was found to approximately follow the dependence $(1 - T^2)$, and this dependence for larger particles (sample 2) transformed and became close to the Bloch law $(1 - T^{3/2})$.

The values of antiferromagnetic susceptibility χ_{AF} obtained as a result of analysis of magnetization curves decrease with increasing temperature similarly to the χ_{AF} dependence in ferritin studied earlier. The extrapolation of $\chi_{AF}(T)$ to high temperatures gives a Néel temperature of 430 K for the samples under study.

The FC hysteresis loop is shifted and this effect increases significantly for the annealed sample. The following specific features of the hysteretic $M(H)$ dependences were revealed: irreversibility up to a field $H = 60$ kOe at $T = 4.2$ K, the passage of the initial magnetization curve outside the hysteresis loop, and different $M(H)$ dependences after field cooling and the repeated cycle of changing an applied field (removal of magnetic prehistory; see Figs. 5a, 5b). These features indicate a significant effect of magnetic anisotropy (jumping of the magnetic moment of a particle over energy barriers after field cooling) on the shift of the hysteresis loop.

The increase in the magnetic moment of the bacterial ferrihydrite particles upon annealing at low temperatures can be used to intentionally change the particle size and to control the magnetic moment of the particles in a rather simple manner. This is important for the practical applications (such as the transport of medicinal agents in an organism) in which particles must be nanosized, have a sufficiently high magnetic moment, and have no magnetization hysteresis at room temperature.

ACKNOWLEDGMENTS

This work was supported by the Ministry of Education and Science of the Russian Federation (state contract in 2014–2016) and a program of the Siberian Branch of the Russian Academy of Sciences.

REFERENCES

1. S. Mørup, D. E. Madsen, C. Fradsen, C. R. H. Bahl, and M. F. Hansen, J. Phys.: Condens. Matter **19**, 213202 (2007).
2. S. P. Gubin, Yu. A. Koshkarov, G. B. Khomutov, and G. Yu. Yurkov, Usp. Khim., No. 6, 539 (2005).
3. R. H. Kodama, J. Magn. Magn. Mater **200**, 359 (1999).
4. Yu. L. Raikher and V. I. Stepanov, J. Exp. Theor. Phys. **107** (3), 435 (2008).
5. L. Néel, C. R. Hebd. Seances Acad. Sci. **252**, 4075 (1961).
6. A. Punnoose, T. Phanthavady, M. S. Seehra, N. Shah, and G. P. Huffman, Phys. Rev. B: Condens. Matter **69**, 054425 (2004).
7. S. A. Makhlouf, F. T. Parker, and A. E. Berkowitz, Phys. Rev. B: Condens. Matter **55**, R14717 (1997).
8. M. S. Seehra, V. S. Babu, A. Manivannan, and J. W. Lynn, Phys. Rev. B: Condens. Matter **61**, 3513 (2000).
9. M. S. Seehra and A. Punnoose, Phys. Rev. B: Condens. Matter **64**, 1132410 (2001).
10. C. Gilles, P. Bonville, H. Rakoto, J. M. Broto, K. K. W. Wong, and S. Mann, J. Magn. Magn. Mater **241**, 430 (2002).
11. N. J. O. Silva, V. S. Amaral, and L. D. Carlos, Phys. Rev. B: Condens. Matter **71**, 184408 (2005).
12. N. J. O. Silva, A. Millan, F. Palacio, E. Kampert, U. Zeitler, and V. S. Amaral, Phys. Rev. B: Condens. Matter **79**, 104405 (2009).
13. S. A. Makhlouf, F. T. Parker, F. E. Spada, and A. E. Berkowitz, J. Appl. Phys. **81**, 5561 (1997).
14. S. A. Makhlouf, H. Al-Attar, and R. H. Kodama, Solid State Commun. **145**, 1 (2008).
15. S. Thota and J. Kumar, J. Phys. Chem. Solids **68**, 1951 (2007).
16. J. F. K. Cooper, A. Ionescu, R. M. Langford, K. R. A. Ziebeck, C. H. W. Barnes, R. Gruar, C. Tighe, J. A. Darr, N. T. K. Thanh, and B. Ouladdiaf, J. Appl. Phys. **114**, 083906 (2013).
17. A. Punnoose and M. S. Seehra, J. Appl. Phys. **91**, 7766 (2002).
18. A. E. Bianchi, S. J. Stewart, R. D. Zysler, and G. Punte, J. Appl. Phys. **112**, 083904 (2012).
19. R. D. Zysler, M. Vasquez Mansilla, and D. Fiorani, Eur. Phys. J. B **41**, 171 (2004).
20. R. D. Zysler, E. Winkler, M. Vasquez Mansilla, and D. Fiorani, Physica B (Amsterdam) **384**, 277 (2006).
21. J. Nogués, J. Sort, V. Langlais, V. Skumryev, S. Suriñach, J. S. Muñoz, and M. D. Baró, Phys. Rep. **422**, 65 (2005).
22. N. J. O. Silva, V. S. Amaral, A. Urtizberea, R. Bustamante, A. Millan, F. Palacio, E. Kampert, U. Zeitler,

S. de Brion, O. Iglesias, and A. Labarta, Phys. Rev. B: Condens. Matter **84**, 104427 (2011).

23. F. Brem, L. Tiefenauer, A. Fink, J. Dobson, and A. M. Hirt, Phys. Rev. B: Condens. Matter **73**, 224427 (2006).
24. J. G. E. Harris, J. E. Grimaldi, D. D. Awschalom, A. Chilero, and D. Loss, Phys. Rev. B: Condens. Matter **60**, 3513 (1999).
25. R. P. Guertin, N. Harrison, Z. X. Zhou, S. McCall, and F. Drymiotis, J. Magn. Magn. Mater. **308**, 97 (2007).
26. S. V. Stolyar, O. A. Bayukov, Yu. L. Gurevich, E. A. Denisova, R. S. Iskhakov, V. P. Ladygina, A. P. Puzyr', P. P. Pustoshilov, and M. A. Bitekhtina, Inorg. Mater. **42** (7), 763 (2006).
27. S. V. Stolyar, O. A. Bayukov, Yu. L. Gurevich, V. P. Ladygina, R. S. Iskhakov, and P. P. Pustoshilov, Inorg. Mater. **43** (6), 638 (2007).
28. M. Balasoiu, S. V. Stolyar, R. S. Iskhakov, L. A. Ischenko, Y. L. Raikher, A. I. Kuklin, O. L. Orelovich, Yu. S. Kovalev, and T. S. Kurkin, Rom. J. Phys. **55**, 782 (2010).
29. Yu. L. Raikher, V. I. Stepanov, S. V. Stolyar, V. P. Ladygina, D. A. Balaev, L. A. Ishchenko, and M. Balasoiu, Phys. Solid State **52** (2), 298 (2010).
30. S. V. Stolyar, O. A. Bayukov, V. P. Ladygina, R. S. Iskhakov, L. A. Ishchenko, V. Yu. Yakovchuk, K. G. Dobretsov, A. I. Pozdnyakov, and O. E. Piksina, Phys. Solid State **53** (1), 100 (2011).
31. D. A. Balaev, A. A. Dubrovskii, A. A. Krasikov, S. V. Stolyar, R. S. Iskhakov, V. P. Ladygina, and E. D. Khilazheva, JETP Lett. **98** (3), 135 (2013).
32. *Mössbauer Mineral Handbook*, Ed. by J. G. Stevens (Mössbauer Effect Data Center, Dalian, China, 2002).
33. A. D. Balaev, Yu. V. Boyarshinov, M. M. Karpenko, and B. P. Khrustalev, Prib. Tekh. Eksp., No. 3, 167 (1985).
34. J. F. Hochepied and M. P. Pileni, J. Appl. Phys. **87**, 2472 (2000).
35. G. F. Goya, T. S. Berquo, F. C. Fonseca, and M. P. Morales, J. Appl. Phys. **94**, 3520 (2003).
36. D. A. Balaev, A. A. Dubrovskiy, K. A. Shaykhutdinov, O. A. Bayukov, S. S. Yakushkin, G. A. Bukhtiyarova, and O. N. Martyanov, J. Appl. Phys. **114**, 163911 (2013).
37. J. P. Chen, C. M. Sorensen, K. J. Klabunde, G. C. Hadjipanayis, E. Devlin, and A. Kostikas, Phys. Rev. B: Condens. Matter **54**, 9288 (1996).
38. C. Martínez-Boubeta, K. Simeonidis, M. Angelakeris, N. Pazos-Pérez, M. Giersig, A. Delimitis, L. Nalbandian, V. Alexandrakis, and D. Niarchos, Phys. Rev. B: Condens. Matter **74**, 054430 (2006).
39. A. B. Drovosekov, N. M. Kreines, D. I. Kholin, A. V. Korolev, M. A. Milyaev, L. N. Romashev, and V. V. Ustinov, JETP Lett. **88** (2), 118 (2008).
40. P. Zhang, F. Zuo, F. K. Urban, A. Khabari, P. Griffiths, and A. Hosseini-Tehrani, J. Magn. Magn. Mater. **225**, 337 (2001).
41. E. Lima, Jr., J. M. Vargas, H. R. Rechenberg, and R. D. Zysler, J. Nanosci. Nanotechnol. **8**, 5913 (2008).
42. D. Fiorani, L. Del Bianco, A. M. Testa, and K. N. Trohidou, J. Phys.: Condens. Matter **19**, 225007 (2007).

Translated by K. Shakhlevich